AIAA JOURNAL
Vol. 45, No. 4, April 2007

Postbuckling Behavior of Angle-Ply Laminated Joined Circular Conical–Cylindrical Shells

S. Singh, B. P. Patel,* and Y. Nath
Indian Institute of Technology Delhi, New Delhi 110 016, India

DOI: 10.2514/1.28358

The prebuckling and the postbuckling behaviors of the angle-ply composite laminated joined circular conical–cylindrical shells subjected to torsion, external pressure, axial compression, and thermal loading are studied considering the variation of stiffness coefficients along the meridional direction in the conical section. The analysis is carried out using the semi-analytical finite element method based on the first-order shear deformation theory. The nonlinear governing equations, derived using Sanders-type kinematic relations, are solved using the Newton–Raphson iterative technique coupled with the displacement control method to trace the prebuckling followed by the postbuckling equilibrium path. The presence of asymmetric perturbation in the form of a small magnitude load spatially proportional to the linear buckling mode shape is considered to initiate the bifurcation of the shell deformation. The influences of the semicone angle, the ply angle, and the number of circumferential waves on the prebuckling/postbuckling response of the angle-ply laminated joined circular conical–cylindrical shells are investigated. The critical buckling load shows a decreasing trend for positive semicone angle cases and an increasing one for negative semicone angle cases with the increase in the magnitude of the semicone angle of the mechanically loaded shells. The shells with a positive semicone angle mostly depict asymmetric bifurcation buckling under uniform decrease in temperature whereas the shells with a negative semicone angle depict asymmetric bifurcation buckling under a uniform rise in temperature. The ratio of the minimum load in the postbuckling path and the critical buckling load may significantly be lower than unity depending upon the shell parameters and loading situations.

Nomenclature

$[\mathbf{A}]$, $[\mathbf{B}]$, $[\mathbf{D}]$	=	matrices of stiffness coefficients
E	=	Young's modulus
$[\mathbf{E}]$	=	matrix of transverse shear stiffness coefficients
$\{\mathbf{F}_M\}$, $\{\mathbf{F}_T\}$	=	mechanical and thermal load vectors
G	=	shear modulus
h	=	total thickness
h_i	=	thickness of ith layer
$[\mathbf{K}]$	=	linear stiffness matrix
$[\mathbf{K}_T]$, $[\mathbf{K}_G]$	=	stiffness matrices due to thermal and initial stress resultants
$[\mathbf{K}_1]$, $[\mathbf{K}_2]$	=	nonlinear stiffness matrices linearly and quadratically dependent on $\{\boldsymbol{\delta}\}$
L	=	length of the shell along the meridional direction
$\{\mathbf{M}\}$, $\{\mathbf{N}\}$	=	moment and stress resultants
$\{\bar{\mathbf{M}}\}$, $\{\bar{\mathbf{N}}\}$	=	thermal moment and stress resultants
N	=	number of layers
n	=	number of circumferential full waves
P	=	axial load
$\{\mathbf{Q}\}$	=	transverse shear stress resultant
q	=	applied external radial pressure
r	=	radius
s, θ, z	=	meridional, circumferential, and thickness coordinates
T	=	torsional load
U	=	total potential energy
u, v, w	=	displacements in the meridional, circumferential, and thickness directions
α	=	coefficient of thermal expansion
β_s, β_θ	=	rotations of the meridional and hoop sections
ΔT	=	temperature rise
$\{\boldsymbol{\delta}\}$	=	degrees of freedom vector
$\{\boldsymbol{\varepsilon}\}$	=	strain vector
θ_i	=	ith layer ply angle
ν	=	Poisson's ratio
ϕ	=	semicone angle

Subcripts

b	=	bending
L, T	=	principal material directions
o	=	middle surface
p	=	extensional/stretching
s	=	shear component of strain/meridional direction
ss, $\theta\theta$	=	normal components in s and θ directions
sz, $s\theta$, θz	=	shear components

Superscripts

c^i	=	coefficient of $\cos(in\theta)$
c^0	=	axisymmetric component
L	=	linear
NL	=	nonlinear
o	=	axisymmetric component/initial state
s^i	=	coefficient of $\sin(in\theta)$
T	=	transpose

I. Introduction

The filament wound laminated conical shells have widespread applications as transition elements between cylinders of different diameters in various engineering fields. Such joined conical–cylindrical shells may often be subjected to torsion, external pressure, axial compression, and thermal loading. A compressive membrane state of stress introduced due to the above loading conditions may lead to the loss of stability by buckling and be a crucial failure phenomenon especially for thin shells. The thin shells may undergo transverse deflections of the order of shell thickness or even higher necessitating the incorporation of the geometric nonlinearity in the problem formulation. An estimate of the critical buckling load can be made through an eigenvalue analysis

Received 16 October 2006; revision received 19 December 2006; accepted for publication 19 December 2006.

*Assistant Professor, Department of Applied Mechanics, Hauz Khas; badripatel@hotmail.com (Corresponding Author).

incorporating either the linear or nonlinear prebuckling states, whereas the sensitivity to imperfections and the postbuckling behavior is evaluated by means of nonlinear analysis. The traditional shell design approach based on the linear bifurcation buckling load reduced by a knockdown factor sometimes may result in overly conservative designs or even potentially unsafe ones. It may be more appropriate to investigate the full nonlinear response of shells and estimate the lowest load in the postbuckling path for design purposes.

The buckling analysis of isotropic joined conical–cylindrical shells has received the attention of a few researchers [1–7]. The elastic buckling and postbuckling analyses of cone–cylinder and sphere–cylinder joined shells subjected to external pressure are investigated by Flores and Godoy [1] using an axisymmetric finite element approach. It is brought out that the bifurcation loads of the joined shells are lower than those of the individual shells, and the former are less imperfection sensitive compared to the latter. The elastic buckling/postbuckling ensuing due to circumferential compressive membrane stress near the intersection of the large end of a cone and a cylinder subjected to internal pressure is also investigated [2–6]. The insertion of a toroidal segment between the cone and cylinder results in slightly higher external buckling pressures than that of a cone–cylinder shell without transition insertion [7].

The studies on the postbuckling characteristics of composite laminated joined conical–cylindrical shells are scarce [8]. The thermoelastic postbuckling characteristics of cross-ply laminated joined conical–cylindrical and conical–cylindrical–conical shells are analyzed in the work of Patel et al. [8] and it is brought out that the behavior of a joined shell system is significantly different from that of the individual components.

The study of angle-ply laminated joined conical–cylindrical shells is important to exploit the tailor making capability of laminated composites. For the continuous fiber wound angle-ply laminated conical shells, layer ply angle and thickness vary along the meridional direction [9–12]. The buckling analysis of angle-ply laminated composite conical shells considering layer ply angle and thickness variation along the meridional direction is dealt with recently by Goldfeld and Arbocz [11] and Goldfeld et al. [12]. It is brought out that the ply angle and the layer thickness are strong functions of the meridional coordinate of an angle-ply laminated conical shell and this in turn, significantly influences the critical buckling loads [11,12]. To the best of the authors' knowledge, there are no studies available on the thermomechanical buckling/postbuckling characteristics of angle-ply laminated joined conical–cylindrical shells.

In the present study, postbuckling characteristics of the angle-ply laminated joined circular conical–cylindrical shells subjected to torsion, external pressure, axial compression, and uniform temperature change are investigated by extending the semi-analytical finite element approach [8] incorporating the variation of the layer ply angle and the thickness along the meridional direction. The presence of the asymmetric perturbation in the form of a small magnitude load spatially proportional to the linear buckling mode shape is considered to initiate the bifurcation of the shell deformation from the axisymmetric mode to the asymmetric one [13]. The solution of the nonlinear governing equations, based on the Sanders type of kinematics, is obtained employing the Newton–Raphson technique and the adaptive displacement control method to efficiently trace the equilibrium path of the shells [8]. The solution starts with the load increments, and whenever during the marching, the tangent stiffness matrix becomes semipositive or negative definite, the solution approach is switched to the adaptive displacement control. The degree of freedom having the highest rate of change in the previous step is selected as the control parameter and is updated in each step. The step size is decided based on the increment in the previous step and the number of equilibrium iterations with suitable error norms. The study is carried out to highlight the influences of the semicone angle, the ply angle, and the number of circumferential waves on the prebuckling/postbuckling response of the angle-ply laminated joined circular conical–cylindrical shells.

II. Formulation

A laminated composite joined circular conical–cylindrical shell is considered as shown in Fig. 1. Based on the first-order shear deformation theory, the displacements u, v, w at a point (s, θ, z) from the median surface are expressed as functions of middle-surface displacements u_o, v_o, and w_o, and rotations β_s and β_θ of the meridional and hoop sections, respectively, as

$$\begin{aligned} u(s,\theta,z) &= u_o(s,\theta) + z\beta_s(s,\theta) \\ v(s,\theta,z) = v_o(s,\theta) + z\beta_\theta(s,\theta); &\qquad w(s,\theta,z) = w_o(s,\theta) \end{aligned} \tag{1}$$

Using the semi-analytical approach, u_o, v_o, w_o, β_s, and β_θ are represented by a Fourier series in the circumferential angle θ. For the nth harmonic, these can be written as

$$\begin{aligned} u_o(s,\theta) &= u_o^{c_0}(s) + \sum_{i=1}^{M_1}\left[u_o^{c_i}(s)\cos(in\theta) + u_o^{s_i}(s)\sin(in\theta)\right] \\ v_o(s,\theta) &= v_o^{c_0}(s) + \sum_{i=1}^{M_1}\left[v_o^{c_i}(s)\cos(in\theta) + v_o^{s_i}(s)\sin(in\theta)\right] \\ w_o(s,\theta) &= w_o^{c_0}(s) + \sum_{i=1}^{M_2}\left[w_o^{c_i}(s)\cos(in\theta) + w_o^{s_i}(s)\sin(in\theta)\right] \\ \beta_s(s,\theta) &= \beta_s^{c_0}(s) + \sum_{i=1}^{M_2}\left[\beta_s^{c_i}(s)\cos(in\theta) + \beta_s^{s_i}(s)\sin(in\theta)\right] \\ \beta_\theta(s,\theta) &= \beta_\theta^{c_0}(s) + \sum_{i=1}^{M_2}\left[\beta_\theta^{c_i}(s)\cos(in\theta) + \beta_\theta^{s_i}(s)\sin(in\theta)\right] \end{aligned} \tag{2}$$

where the superscript c_0 refers to the axisymmetric component of displacement field variables, and c_i and s_i $(i \geq 1)$ refer to the asymmetric components of the field variables having the circumferential variation proportional to $\cos(in\theta)$ and $\sin(in\theta)$, respectively.

The strain-displacement relations are based on Sanders [14] type of kinematic approximations: 1) small strains, 2) moderately large rotations about the axes tangent to the middle surface, 3) effect of rotation about normal to the middle surface is negligible; and 4) thin shell $(z/r \ll 1)$ such that $1 + z/r \approx 1$; however, transverse shear deformation is important due to a smaller wavelength of the postbuckling deformation to thickness ratio and higher E/G ratio. The Green's strains are written in terms of the midsurface deformations as

$$\{\boldsymbol{\varepsilon}\} = \begin{Bmatrix} \boldsymbol{\varepsilon}_p^L \\ 0 \end{Bmatrix} + \begin{Bmatrix} z\boldsymbol{\varepsilon}_b \\ \boldsymbol{\varepsilon}_s \end{Bmatrix} + \begin{Bmatrix} \boldsymbol{\varepsilon}_p^{\mathrm{NL}} \\ 0 \end{Bmatrix} \tag{3}$$

where the membrane strains $\{\boldsymbol{\varepsilon}_p^L\}$, bending strains $\{\boldsymbol{\varepsilon}_b\}$, shear strains $\{\boldsymbol{\varepsilon}_s\}$, and the nonlinear in-plane strains $\{\boldsymbol{\varepsilon}_p^{\mathrm{NL}}\}$ in Eq. (3) are written as [14,15]

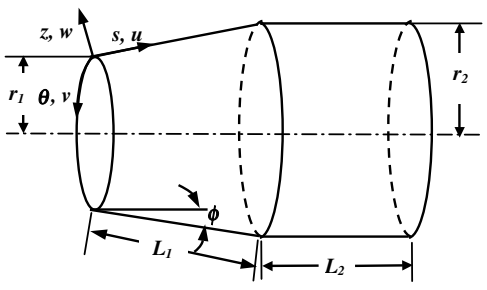

Fig. 1 Coordinate system and geometrical details of joined conical–cylindrical shell.

$$\{\boldsymbol{\varepsilon}_p^L\} = \begin{Bmatrix} \frac{\partial u_o}{\partial s} \\ \frac{u_o \sin\phi}{r} + \frac{\partial v_o}{r\partial\theta} + \frac{w_o \cos\phi}{r} \\ \frac{\partial u_o}{r\partial\theta} - \frac{v_o \sin\phi}{r} + \frac{\partial v_o}{\partial s} \end{Bmatrix}; \qquad \{\boldsymbol{\varepsilon}_b\} = \begin{Bmatrix} \frac{\partial \beta_s}{\partial s} \\ \frac{\beta_s \sin\phi}{r} + \frac{\partial \beta_\theta}{r\partial\theta} \\ \frac{\partial \beta_s}{r\partial\theta} + \frac{\partial \beta_\theta}{\partial s} - \frac{\beta_\theta \sin\phi}{r} \end{Bmatrix}$$

$$\{\boldsymbol{\varepsilon}_s\} = \begin{Bmatrix} \beta_s + \frac{\partial w_o}{\partial s} \\ \beta_\theta + \frac{\partial w_o}{r\partial\theta} - \frac{v_o \cos\phi}{r} \end{Bmatrix}; \qquad \{\boldsymbol{\varepsilon}_p^{\mathrm{NL}}\} = \begin{Bmatrix} \frac{1}{2}\left(\frac{\partial w_o}{\partial s}\right)^2 \\ \frac{1}{2}\left(\frac{\partial w_o}{r\partial\theta} - \frac{v_0 \cos\phi}{r}\right)^2 \\ \frac{\partial w_o}{\partial s}\left(\frac{\partial w_o}{r\partial\theta} - \frac{v_0 \cos\phi}{r}\right) \end{Bmatrix} \tag{4}$$

The stress resultant vector $\{\mathbf{N}\} = \{N_{ss} N_{\theta\theta} N_{s\theta}\}^T$ and the moment resultant vector $\{\mathbf{M}\} = \{M_{ss} M_{\theta\theta} M_{s\theta}\}^T$ can be expressed in terms of the membrane strains $\{\boldsymbol{\varepsilon}_p\} = \{\boldsymbol{\varepsilon}_o^L\} + \{\boldsymbol{\varepsilon}_o^{\mathrm{NL}}\}$ and the bending strains $\{\boldsymbol{\varepsilon}_b\}$ through the constitutive relations as

$$\begin{Bmatrix} \{\mathbf{N}\} \\ \{\mathbf{M}\} \end{Bmatrix} = \begin{bmatrix} [\mathbf{A}] & [\mathbf{B}] \\ [\mathbf{B}] & [\mathbf{D}] \end{bmatrix} \begin{Bmatrix} \{\varepsilon_p\} \\ \{\varepsilon_b\} \end{Bmatrix} - \begin{Bmatrix} \{\bar{\mathbf{N}}\} \\ \{\bar{\mathbf{M}}\} \end{Bmatrix} \tag{5}$$

The transverse shear stress resultant vector $\{\mathbf{Q}\} = \{Q_{sz}\ Q_{\theta z}\}^T$ is related to the transverse shear strain $\{\boldsymbol{\varepsilon}_s\}$ through the constitutive relation as

$$\{\mathbf{Q}\} = [\mathbf{E}]\{\boldsymbol{\varepsilon}_s\} \tag{6}$$

It may be noted here that the stiffness coefficients [**A**], [**D**], [**B**], and [**E**] used in Eqs. (5) and (6) are functions of the meridional coordinate (s).

For a laminated shell consisting of N layers with the stacking angles $\theta_i (i = 1, \ldots, N)$ and the layer thicknesses $h_i (i = 1, \ldots, N)$, the necessary expressions to compute the stiffness coefficients and the thermal stress/moment resultants, available in the literature [16], are used.

The variation of the ply angle θ_i and the layer thickness h_i for the filament wound laminated conical section is expressed as [11,12]

$$\theta_i = \arcsin\left(\frac{r_1}{r}\ \sin\theta_i^1\right) \tag{7a}$$

$$h_i = h_i^1 \frac{r_1}{r} \frac{\cos\theta_i^1}{\cos\theta_i} \tag{7b}$$

where r_1, θ_i^1, and h_i^1 are the radius of the parallel circle, the ply angle, and the layer thickness at the left end of the shell. The potential energy functional $U_1(\boldsymbol{\delta})$ (consisting of strain energy and potential of external loads) is given by

$$U_1(\boldsymbol{\delta}) = \frac{1}{2}\int_A \left[\begin{Bmatrix} \boldsymbol{\varepsilon}_p \\ \boldsymbol{\varepsilon}_b \end{Bmatrix}^T \begin{bmatrix} \mathbf{A} & \mathbf{B} \\ \mathbf{B} & \mathbf{D} \end{bmatrix} \begin{Bmatrix} \boldsymbol{\varepsilon}_p \\ \boldsymbol{\varepsilon}_b \end{Bmatrix} + \{\boldsymbol{\varepsilon}_s\}^T [\mathbf{E}] \{\boldsymbol{\varepsilon}_s\} - \begin{Bmatrix} \boldsymbol{\varepsilon}_p \\ \boldsymbol{\varepsilon}_b \end{Bmatrix}^T \begin{Bmatrix} \bar{\mathbf{N}} \\ \bar{\mathbf{M}} \end{Bmatrix} \right] \mathrm{d}A - \int_A q w_o \, \mathrm{d}A - v_o^{c_0}(0) T - u_o^{c_0}(0) P \tag{8}$$

where T and P are applied at the left end ($s = 0$) of the shell.

The potential energy $U_2(\boldsymbol{\delta})$ due to the initial state of in-plane stress resultants is written as

$$U_2(\boldsymbol{\delta}) = \int_A \left\{\boldsymbol{\varepsilon}_p^{\mathrm{NL}}\right\}^T \{\mathbf{N}^0\} \, \mathrm{d}A \tag{9}$$

Following the procedure of Rajasekaran and Murray [17], the total potential energy functional $U(\boldsymbol{\delta})[= U_1(\boldsymbol{\delta}) + U_2(\boldsymbol{\delta})]$ can be expressed as

$$U(\boldsymbol{\delta}) = \{\boldsymbol{\delta}\}^T [(1/2)[[\mathbf{K}] - [\mathbf{K}_T] + [\mathbf{K}_G]] + (1/6)[\mathbf{K}_1(\boldsymbol{\delta})] + (1/12)[\mathbf{K}_2(\boldsymbol{\delta})]]\{\boldsymbol{\delta}\} - \{\boldsymbol{\delta}\}^T \{\mathbf{F}_M\} - \{\boldsymbol{\delta}\}^T \{\mathbf{F}_T\} \tag{10}$$

The condition for the extremum of $U(\boldsymbol{\delta})$ with respect to $\boldsymbol{\delta}$ leads to the governing equations of the shell as

$$[[\mathbf{K}] - [\mathbf{K}_T] + [\mathbf{K}_G] + (1/2)[\mathbf{K}_1(\boldsymbol{\delta})] + (1/3)[\mathbf{K}_2(\boldsymbol{\delta})]]\{\boldsymbol{\delta}\} = \{\mathbf{F}_M\} + \{\mathbf{F}_T\} \tag{11}$$

The governing Eq. (11) can be employed to study the linear/nonlinear static and the eigenvalue buckling analyses by neglecting the appropriate terms such as the following:

Linear static analysis:

$$[\mathbf{K}]\{\boldsymbol{\delta}\} = \{\mathbf{F}_M\} + \{\mathbf{F}_T\} \tag{12}$$

Nonlinear static analysis:

$$[[\mathbf{K}] - [\mathbf{K}_T] + (1/2)[\mathbf{K}_1(\boldsymbol{\delta})] + (1/3)[\mathbf{K}_2(\boldsymbol{\delta})]]\{\boldsymbol{\delta}\} = \{\mathbf{F}_M\} + \{\mathbf{F}_T\} \tag{13}$$

Eigenvalue buckling analysis:

$$[\mathbf{K}]\{\boldsymbol{\delta}\} = \lambda[\mathbf{K}_G^*]\{\boldsymbol{\delta}\} \tag{14}$$

where $[\mathbf{K}_G^*]$ is the geometric stiffness due to the initial state of stress developed because of the unit load and λ is the load multiplier factor. It may be noted here that for the purpose of evaluating $[\mathbf{K}_G^*]$, first the static analysis of the shell using Eq. (12) for the unit load is carried out. The resulting deformation field is used to calculate the initial state of stress resultants using Eq. (5) and in turn, for evaluating the $[\mathbf{K}_G^*]$ matrix.

The nonlinear equilibrium path is traced by solving Eq. (13) using the Newton–Raphson iteration technique coupled with the adaptive displacement control method. The equilibrium is achieved for each load/displacement step until the convergence criteria suggested by Bergan and Clough [18] are satisfied within the specific tolerance limit of less than 0.001%.

The detailed description of the finite element formulation and its validation for buckling/postbuckling studies of cross-ply laminated shells can be found elsewhere [8,19,20] and are not presented here for the sake of brevity.

III. Results and Discussion

The nonlinear prebuckling and the postbuckling characteristics of the angle-ply laminated joined circular conical–cylindrical shells are investigated using the semi-analytical finite element formulation. The presence of the small magnitude initial disturbance in the form of a radial load spatially proportional to the linear buckling mode shape is considered to trace the postbuckling path. The disturbance load amplitude corresponds to a maximum transverse displacement parameter $\bar{w}_{o\max}/h = 0.001$ in the linear static analysis of the shell subjected only to the disturbance load. The influence of the small asymmetric disturbance on the prebuckling deformation of the axisymmetrically loaded shell is very small and when the applied axisymmetric load approaches the bifurcation load, the solution continues to the postbuckling path. The detailed study is carried out to highlight the influences of the semicone angle (ϕ), the ply angle (θ_i^1), and the number of circumferential waves (n) on the prebuckling/postbuckling characteristics of the angle-ply laminated joined circular conical–cylindrical shells.

The material properties used, unless otherwise specified, are $E_L = 172.25$ GPa, $E_T = 6.89$ GPa, $G_{LT} = 3.445$ GPa, $G_{TT} = 1.378$ GPa, $\nu_{LT} = \nu_{TT} = 0.25$, $\alpha_L = 6.3 \times 10^{-6}/^\circ$C, and $\alpha_T = 3\alpha_L$. The subscripts L and T are the longitudinal and the transverse directions, respectively, with respect to the fibers. All the layers are of equal thickness at the left end ($s = 0$) and the ply angle is measured with respect to the meridional axis (s axis). The first layer is the innermost layer of the shell. The layer ply angle (θ_i^1) and thickness h_i^1 at the left end ($s = 0$) of the shell are specified. The shear correction factor employed is evaluated taking into account layer properties and stacking sequence [21].

The simply supported boundary conditions of the shells considered are the following:

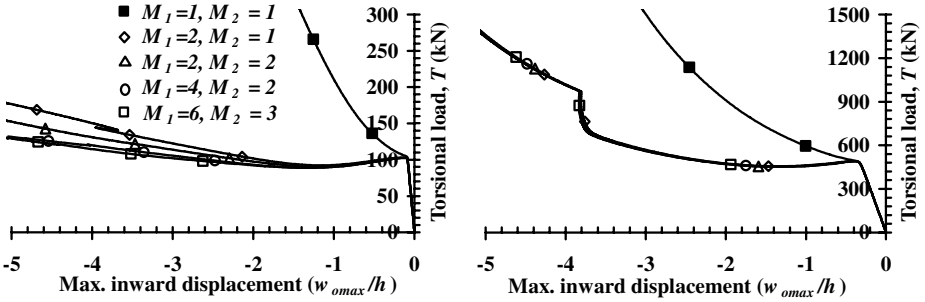

Fig. 2 Convergence study for two-layered angle-ply laminated joined conical–cylindrical shells ($L_2/r_2 = 1$, $r_2/h = 100$, $L_1 = L_2$): a) 15 deg / −15 deg, $\phi = 30$ deg, $n = 13$; b) 15 deg / −15 deg, $\phi = -30$ deg, $n = 13$.

1) Right end ($s = L$)

$$u_o^{c_0} = u_o^{c_i} = u_o^{s_i} = v_o^{c_i} = v_o^{s_i} = w_o^{c_0} = w_o^{c_i} = w_o^{s_i} = \beta_\theta^{c_0} = \beta_\theta^{c_i} = \beta_\theta^{s_i} = M_{ss} = 0 \tag{15}$$

2) Left end ($s = 0$)

Torsional loading:

$$\text{Immovable: } u_o^{c_0} = u_o^{c_i} = u_o^{s_i} = v_o^{c_i} = v_o^{s_i} = w_o^{c_0} = w_o^{c_i} = w_o^{s_i} = \beta_\theta^{c_0} = \beta_\theta^{c_i} = \beta_\theta^{s_i} = M_{ss} = 0 \tag{16}$$

External radial/axial/thermal loading:

$$\text{Immovable: } u_o^{c_0} = u_o^{c_i} = u_o^{s_i} = v_o^{c_0} = v_o^{c_i} = v_o^{s_i} = w_o^{c_0} = w_o^{c_i} = w_o^{s_i} = \beta_\theta^{c_0} = \beta_\theta^{c_i} = \beta_\theta^{s_i} = M_{ss} = 0 \tag{17}$$

$$\text{Movable: } u_o^{c_i} = u_o^{s_i} = v_o^{c_0} = v_o^{c_i} = v_o^{s_i} = w_o^{c_0} = w_o^{c_i} = w_o^{s_i} = \beta_\theta^{c_0} = \beta_\theta^{c_i} = \beta_\theta^{s_i} = M_{ss} = 0 \tag{18}$$

Based on the progressive mesh refinement, 48 elements idealization in the meridional direction is found to be adequate to model the complete slant length of the joined shell. The number of terms M_1 in the approximation of the variables (u_o, v_o) and M_2 in (w_o, β_s, β_θ), based on the convergence study (one typical result is shown in Fig. 2), are taken as 4 and 2, respectively, for the detailed parametric study. The validation of the formulation for the buckling of the angle-ply laminated conical shells considering the variation of the ply angle and the layer thickness along the meridional direction is carried out and the results are shown in Table 1. It can be seen from Table 1 that the present results are in good agreement with those available in the literature [11]. The comparison of the results for the postbuckling characteristics of angle-ply laminated cylindrical shells ($\phi = 0$ deg) with those of Sheinman and Jabareen [22] is given in Fig. 3 and is found to be in quite good agreement. Some differences in the results, as seen in Fig. 3b, may be attributed to a different shell theory and solution approach employed by Sheinman and Jabareen

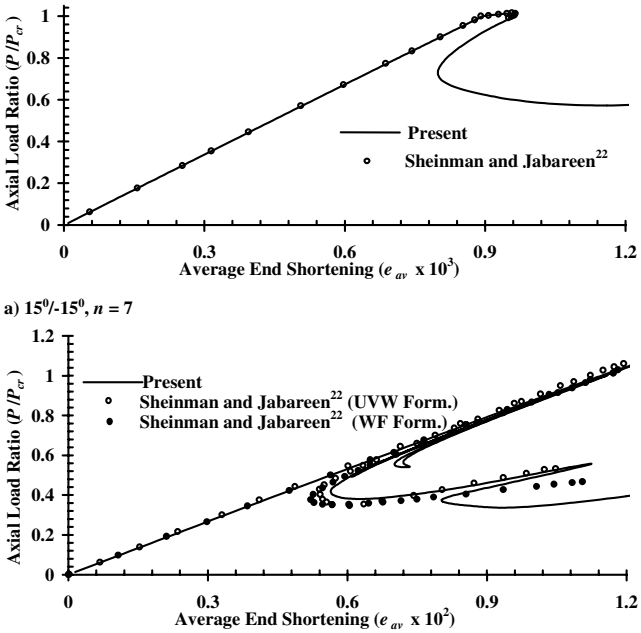

Fig. 3 Comparison of postbuckling characteristics of an angle-ply ($\theta^1/-\theta^1$) laminated circular cylindrical shell subjected to axial compression $L/r = 2, r/h = 100, h = 0.0127$ m; $E_L = 140.4$ GPa, $E_T = 9.73$ GPa $G_{LT} = G_{TT} = 4.11$ GPa, $\nu_{LT} = \nu_{TT} = 0.26$; boundary conditions at right end ($s = L$): $u_o = v_o = w_o = \beta_s = \beta_\theta = 0$, at left end ($s = 0$): $w_o = \beta_s = \beta_\theta = 0$, $v_o = 0$ for $\theta^1 = 15$ deg and $v_o \neq 0$ for $\theta^1 = 60$ deg.

[22]. It can further be seen from Fig. 3b that the present analysis predicts the presence of multiple loops in the postbuckling path predicted using the adaptive displacement control method employed in the paper. This method can accurately trace the continuously

Table 1 Comparison of critical buckling loads for angle-ply laminated circular conical shell [$L = 0.2$ m, $r_1 = 0.1325$ m, total thickness at small end: $h_1 = 1.16$ mm, lamination scheme at small end: 90 deg /45 deg / −45 deg /90 deg; $E_L = 42.6$ GPa, $E_T = 11.7$ GPa, $G_{LT} = G_{TT} = 4.8$ GPa, $\nu_{LT} = \nu_{TT} = 0.302$; boundary conditions at large end ($s = L$): $u_o = v_o = w_o = \beta_\theta = 0$, at small end ($s = 0$): $w_o = \beta_\theta = 0$, $v_o = 0$ (axial load case), $u_o = v_o = 0$ (external pressure), $u_o = 0$ (torsional)]

	Critical axial load, P_{cr}, kN/m		Critical external pressure, p_{cr}. kN/m^2		Critical torsional load, T_{cr}, kN/m	
ϕ	Present	Goldfeld and Arbocz [11]	Present	Goldfeld and Arbocz [11]	Present	Goldfeld and Arbocz [11]
0 deg	106.72	106.89	170.67	179.83	46.78	46.18
10 deg	75.10	74.54	108.98	113.82	43.24	——
20 deg	58.97	59.18	73.043	75.962	40.56	——
30 deg	48.24	48.13	49.289	51.136	38.15	37.80
45 deg	35.63	35.38	26.136	27.047	32.66	32.37
55 deg	27.99	27.83	15.967	16.466	27.68	27.51
65 deg	20.55	20.42	8.6854	8.8947	21.87	21.71
75 deg	12.82	12.66	3.6252	3.6881	15.07	14.99
85 deg	4.097	——	0.6292	0.6335	7.108	7.016
90 deg	0.508	0.508	——	——	3.131	——

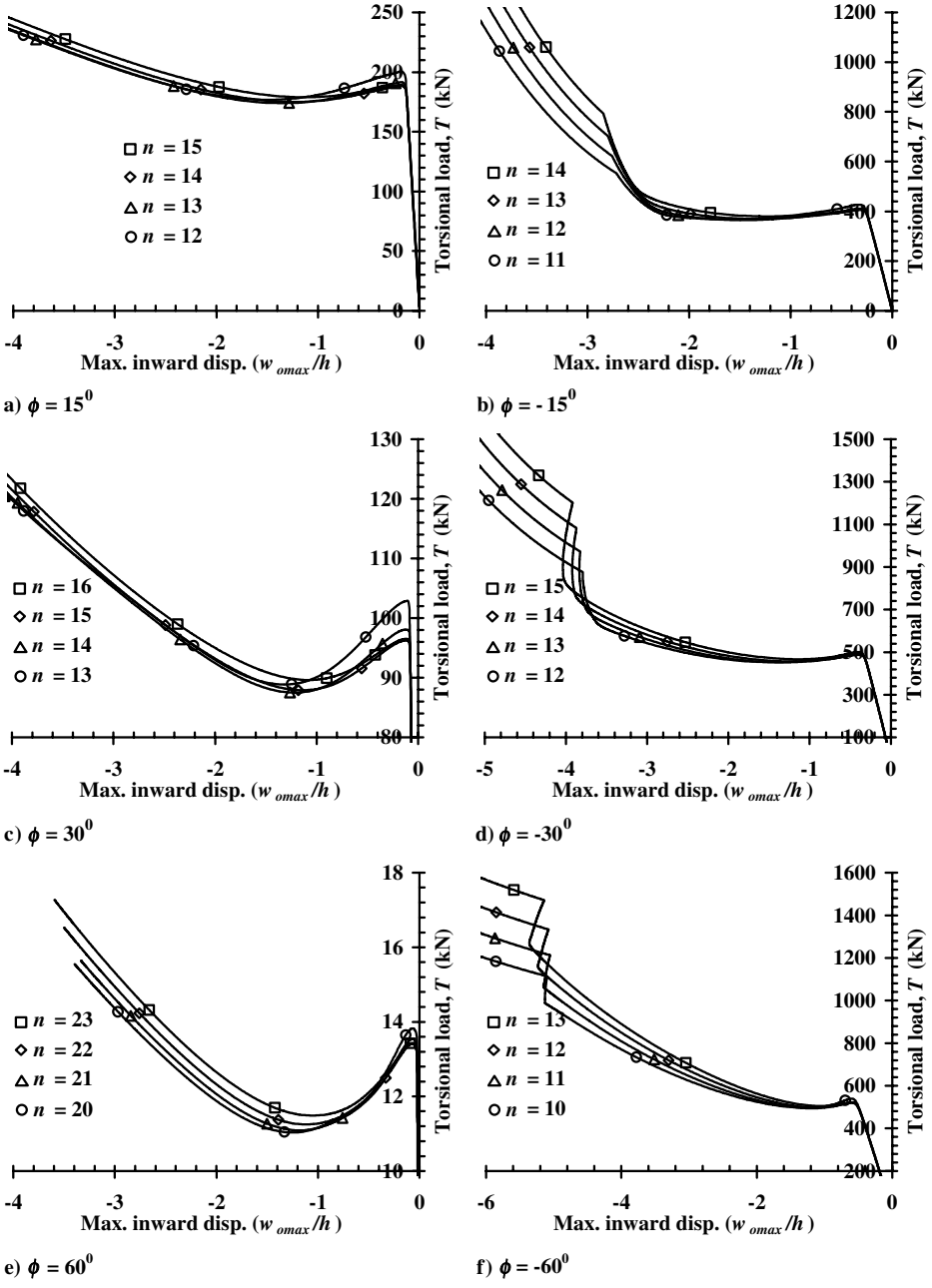

Fig. 4 Nonlinear response curves for two-layered (15 deg / − 15 deg) angle-ply laminated immovable simply supported joined conical–cylindrical shells subjected to torsional load at the left end.

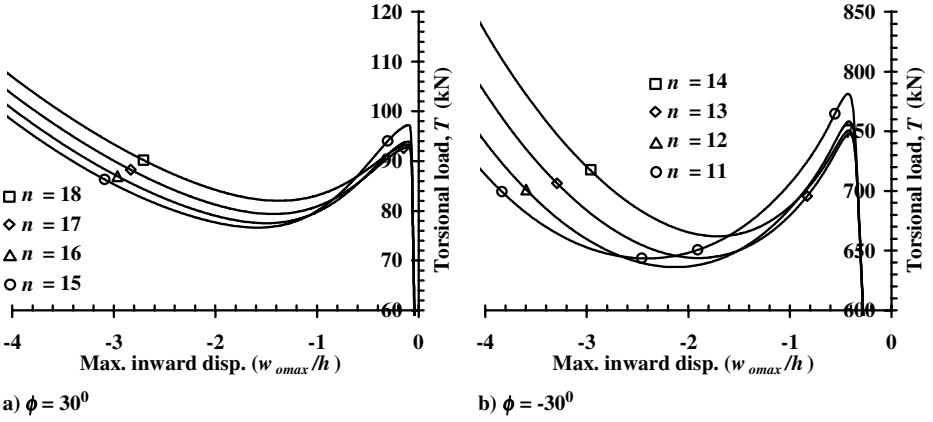

Fig. 5 Nonlinear response curves for two-layered (30 deg / − 30 deg) angle-ply laminated immovable simply supported joined conical–cylindrical shells subjected to torsional load at the left end.

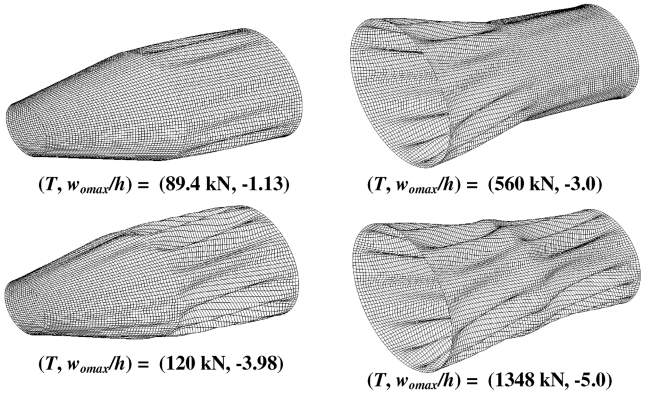

Fig. 6 Postbuckling deformation shapes for 15 deg / − 15 deg shell subjected to torsional load ($n = 13$).

connected branches/loops of the equilibrium path. The presence of such multiple loops near the bifurcation point of structures is similar to that highlighted in the literature [23].

The postbuckling characteristics of the two-layered angle-ply $(\theta^1/-\theta^1)$ laminated immovable simply supported joined conical–cylindrical shells ($L_1/r_1 = 1$, $r_1/h = 100$, $L_1 = L_2$, $h = 0.003$ m) subjected to the torsional load T at the left end are shown in Figs. 4 and 5 for the ply angles $\theta^1 = 15$ deg and 30 deg, respectively, considering different values of the positive and negative semicone angles of the conical section. The circumferential wave numbers (n) correspond to the lowest critical load and in its neighborhood. It can be observed from these figures that the maximum inward transverse displacement parameter $(w_{o\max}/h)$ increases almost linearly with the increase in the torque up to a certain critical value beyond which the equilibrium path reveals bifurcation from the axisymmetric deformation to the combination of the axisymmetric and the asymmetric deformation with the dominance of the latter one. The

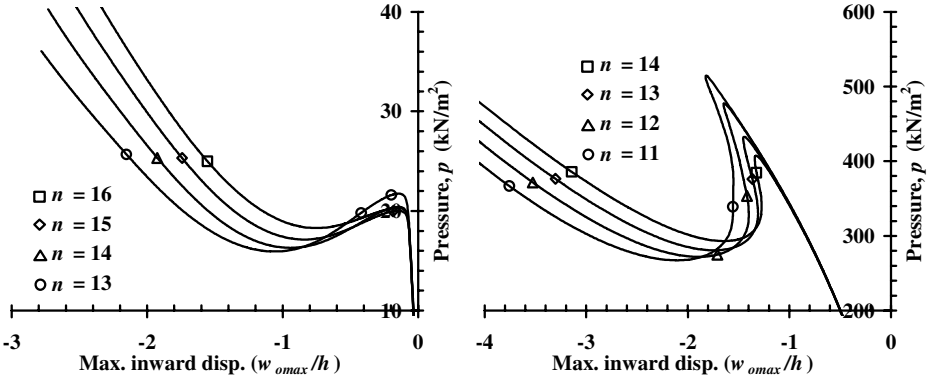

Fig. 7 Nonlinear response curves for two-layered (30 deg / − 30 deg) angle-ply laminated immovable simply supported joined conical–cylindrical shells subjected to radial external pressure.

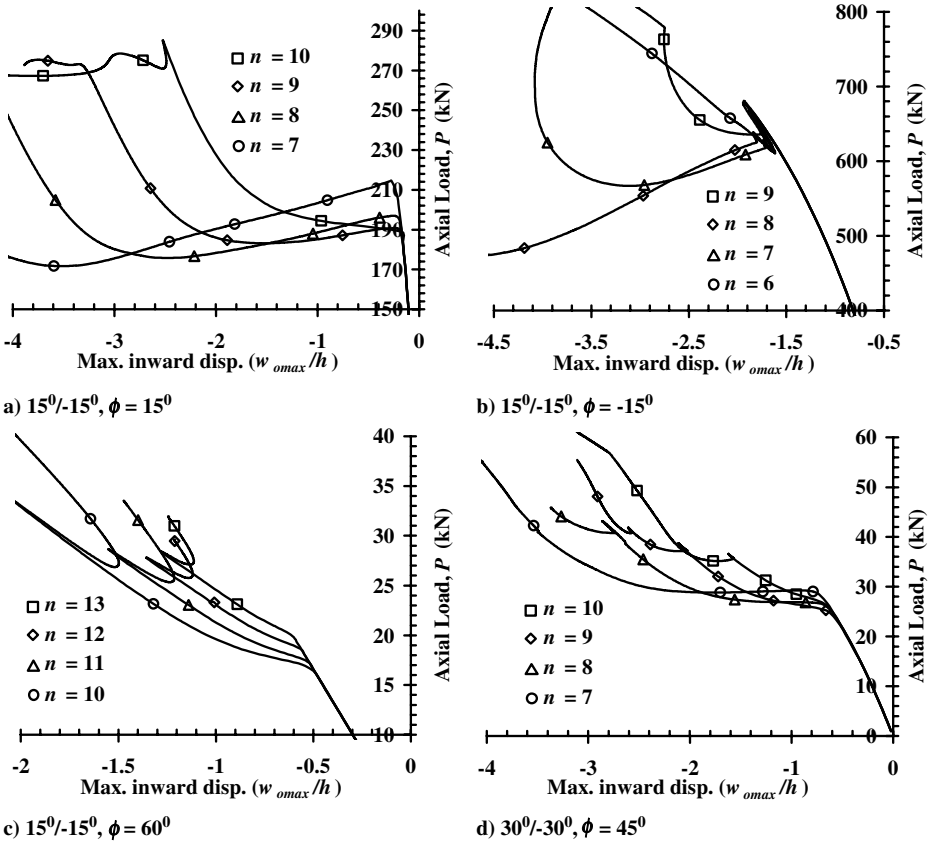

Fig. 8 Nonlinear response curves for two-layered angle-ply laminated movable simply supported joined conical–cylindrical shells subjected to axial compressive load at the left end.

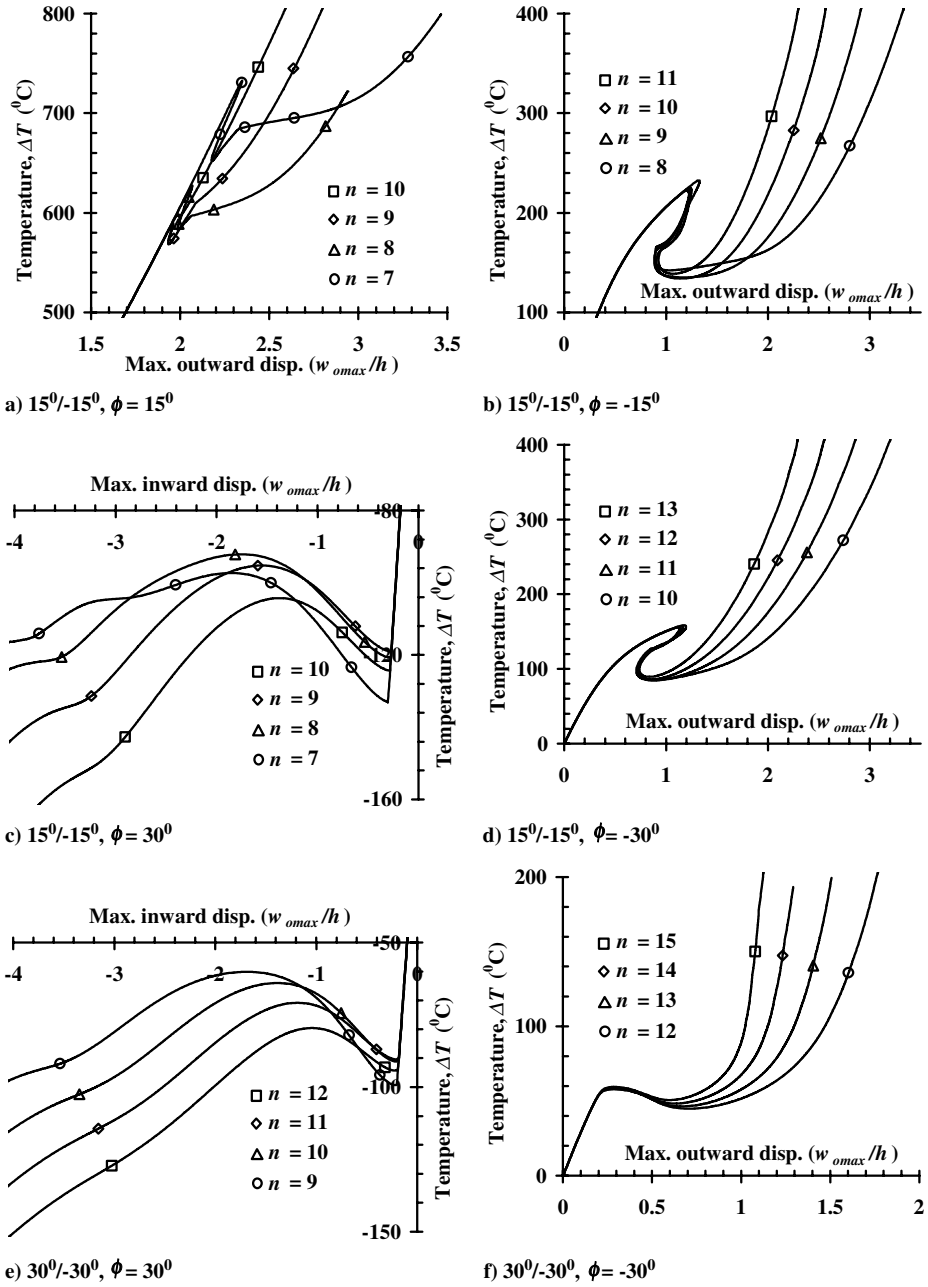

Fig. 9 Nonlinear response curves for two-layered angle-ply laminated immovable simply supported joined conical–cylindrical shells exposed to uniform temperature change.

critical torsional load decreases with the increase in the positive semicone angle whereas it increases with the increase in the magnitude of the negative semicone angle. The rate of change of critical torsional load is more for the positive semicone angle shell cases. The circumferential wave number corresponding to the minimum load ($T_{\min}$) in the postbuckling path is lower than the one corresponding to the lowest buckling load ($T_{\rm cr}$). The ratio $T_{\min}/T_{\rm cr}$ is more for ply angle $\theta^1 = 15$ deg compared to $\theta^1 = 30$ deg for a particular value of ϕ. It can also be inferred from Figs. 4 and 5 that the degree of the hardening nonlinearity, depicted after the minimum load in the postbuckling path, increases with the increase in the circumferential wave number. The 15 deg / − 15 deg shells with a negative semicone angle reveal secondary bifurcation in the postbuckling path (Fig. 4). The typical postbuckling deformation shapes for 15 deg / − 15 deg shells shown in Fig. 6 reveal that the buckling first initiates in the cylindrical section for $\phi = 30$ deg and in the conical section for $\phi = -30$ deg.

The behavior of the angle-ply $(\theta^1/-\theta^1)$ laminated immovable simply supported conical–cylindrical shells subjected to the external radial pressure is qualitatively similar to that of the shells subjected to the torsional loading. The typical characteristics are shown in Fig. 7 for $\theta^1 = 30$ deg. It can be seen from Fig. 7 that the prebuckling displacement corresponding to the buckling point is significantly higher for shells with a negative semicone angle.

The response characteristics of the shells subjected to the axial compressive load are depicted in Fig. 8. It can be seen from this figure that the shells with lower semicone angle (ϕ) magnitude reveal significantly lower $P_{\min}/P_{\rm cr}$ ratio whereas the shells with higher ϕ exhibit a rising initial postbuckling path. One can also see from Fig. 8 that the joined shells subjected to axial loading exhibit secondary bifurcation for most of the shell parameters.

The detailed study is also carried out for the angle-ply $(\theta^1/-\theta^1)$ laminated conical–cylindrical shells subjected to the uniform change in temperature. The typical results are presented in Fig. 9 for the ply angle $\theta^1 = 15$ deg and 30 deg. It is revealed from the detailed study that the shells with a positive semicone angle except for the case $(\theta^1, \phi) = (15 \text{ deg}, 15 \text{ deg})$ depict asymmetric bifurcation buckling due to cooling (decrease in temperature from their undeformed/

unstressed equilibrium temperature) whereas the shells with a negative semicone angle depict asymmetric bifurcation buckling due to heating (rise in temperature) for the shell parameters considered. The shell with $\theta^1 = 15$ deg and $\phi = 15$ deg reveals asymmetric buckling under both the conditions (the results for a decrease in the temperature case for $\theta^1 = 15$ deg and $\phi = 15$ deg are not shown). It is apt to make a mention here that the linear eigenvalue analysis also predicts positive buckling temperature significantly higher compared to negative buckling temperature for the angle-ply shells with a positive semicone angle conical section. However, the nonlinear analysis of such shells may not predict bifurcation from axisymmetric prebuckling to asymmetric buckling depending upon the level of buckling temperature rise. It is expected that the buckling/postbuckling study of the joined conical–cylindrical shells subjected to thermal heating/cooling will be useful in the analysis/design of storage tanks/shells for cryogenic/low-temperature applications.

IV. Conclusions

The prebuckling and the postbuckling characteristics of the angle-ply laminated joined circular conical–cylindrical shells subjected to the mechanical and thermal loading are analyzed employing the semi-analytical finite element. The detailed study revealed that the critical buckling load shows a decreasing trend with the increase in the positive semicone angle and an increasing one with the increase in the magnitude of the negative semicone angle for mechanical loading situations. However, the critical buckling temperature decreases for both cases. In general, the shells with a positive semicone angle depict asymmetric bifurcation buckling under a decrease in temperature from their undeformed/unstressed equilibrium temperature, whereas the shells with a negative semicone angle depict asymmetric bifurcation buckling under a rise in temperature. The circumferential wave number corresponding to the minimum load in the postbuckling path is lower than the one corresponding to the lowest buckling load. The ratio of the minimum load in the postbuckling path and the critical buckling load may significantly be lower than unity depending upon the shell parameters and loading situations.

References

[1] Flores, F. G., and Godoy, L. A., "Postbuckling of Elastic Cone-Cylinder and Sphere-Cylinder Complex Shells," *International Journal of Pressure Vessels and Piping*, Vol. 45, No. 2, 1991, pp. 237–258.

[2] Teng, J. G., "Cone-Cylinder Intersection Under Internal Pressure: Axisymmetric Failure," *Journal of Engineering Mechanics*, Vol. 120, No. 9, 1994, pp. 1896–1912.

[3] Teng, J. G., "Cone-Cylinder Intersection Under Internal Pressure: Nonsymmetric Buckling," *Journal of Engineering Mechanics*, Vol. 121, No. 12, 1995, pp. 1298–1305.

[4] Teng, J. G., "Elastic Buckling of Cone-Cylinder Intersection Under Localized Circumferential Compression," *Engineering Structures*, Vol. 18, No. 1, 1996, pp. 41–48.

[5] Teng, J. G., and Ma, H.-W., "Elastic Buckling of Ring-Stiffened Cone-Cylinder Intersections Under Internal Pressure," *International Journal of Mechanical Sciences*, Vol. 41, No. 11, 1999, pp. 1357–1383.

[6] Zhao, Y., and Teng, J. G., "A Stability Design Proposal for Cone-Cylinder Intersections Under Internal Pressure," *International Journal of Pressure Vessels and Piping*, Vol. 80, No. 5, 2003, pp. 297–309.

[7] Anwen, W., "Stresses and Stability for the Cone-Cylinder Shells with Toroidal Transition," *International Journal of Pressure Vessels and Piping*, Vol. 75, No. 1, 1998, pp. 49–56.

[8] Patel, B. P., Nath, Y., and Shukla, K. K., "Nonlinear Thermo-Elastic Buckling Characteristics of Cross-Ply Laminated Joined Conical-Cylindrical Shells," *International Journal of Solids and Structures*, Vol. 43, No. 16, 2006, pp. 4810–4829.

[9] Baruch, M., Arbocz, J., and Zhang, G. Q., "Laminated Conical Shells—Considerations For The Variations of The Stiffness Coefficients," *Proceedings of the 36th AIAA/ASME/ASCE/AHS/ASC, S. S. D. M. Conference*, AIAA, Reston, VA, 1994, pp. 2505–2516.

[10] Korjakin, A., Rikards, R., Chate, A., and Altenbach, H., "Analysis of Free Damped Vibrations of Laminated Composite Conical Shells," *Composite Structures*, Vol. 41, No. 1, 1998, pp. 39–47.

[11] Goldfeld, Y., and Arbocz, J., "Buckling of Laminated Conical Shells Given The Variations of The Stiffness Coefficients," *AIAA Journal*, Vol. 42, No. 3, 2004, pp. 642–649.

[12] Goldfeld, Y., Arbocz, J., and Rothwell, A., "Design and Optimization of Laminated Conical Shells For Buckling," *Thin-Walled Structures*, Vol. 43, No. 1, 2005, pp. 107–133.

[13] Teng, J. G., and Song, C. Y., "Numerical Models for Nonlinear Analysis of Elastic Shells with Eigenmode-Affine Imperfections," *International Journal of Solids and Structures*, Vol. 38, No. 18, 2001, pp. 3263–3280.

[14] Sanders, J. L., "Nonlinear Theories For Thin Shells," *Quarterly of Applied Mathematics*, Vol. 21, No. 1, 1963, pp. 21–36.

[15] Kraus, H., *Thin Elastic Shells*, Wiley, New York, 1976.

[16] Jones, R. M., *Mechanics of Composite Materials*, Taylor and Francis, Philadelphia, PA, 1999.

[17] Rajasekaran, S., and Murray, D. W., "Incremental Finite Element Matrices," *Journal of the Structural Division*, Vol. 99, No. ST12, 1973, pp. 2423–2438.

[18] Bergan, P. G., and Clough, R. W., "Convergence Criteria For Iterative Process," *AIAA Journal*, Vol. 10, No. 8, 1972, pp. 1107–1108.

[19] Patel, B. P., Shukla, K. K., and Nath, Y., "Thermal Postbuckling Characteristics of Laminated Conical Shells with Temperature Dependent Material Properties," *AIAA Journal*, Vol. 43, No. 6, 2005, pp. 1380–1388.

[20] Patel, B. P., Shukla, K. K., and Nath, Y., "Thermal Postbuckling Analysis of Laminated Cross-Ply Truncated Circular Conical Shells," *Composite Structures*, Vol. 71, No. 1, 2005, pp. 101–114.

[21] Vlachoutsis, S., "Shear Correction Factors for Plates and Shells," *International Journal for Numerical Methods in Engineering*, Vol. 33, No. 7, 1992, pp. 1537–1552.

[22] Sheinman, I., and Jabareen, M., "Postbuckling of Laminated Cylindrical Shells in Different Formulations," *AIAA Journal*, Vol. 43, No. 5, 2005, pp. 1117–1123.

[23] El Naschie, M. S., *Stress, Stability and Chaos in Structural Engineering: An Energy Approach*, McGraw–Hill, London, 1992.

A. Palazotto
Associate Editor